Effects of shock-breakout pressure on ejection of micron-scale material from shocked tin surfaces

M. B. Zellner[a)]
P-23, Los Alamos National Laboratory, P.O. Box 1663, Los Alamos, New Mexico 87545

M. Grover
Special Technologies Laboratory, 6159 Keister Place, Goleta, California 93117

J. E. Hammerberg
X-1-SMMP, Los Alamos National Laboratory, P.O. Box 1663, Los Alamos, New Mexico 87545

R. S. Hixson
DE-DO, Los Alamos National Laboratory, P.O. Box 1663, Los Alamos, New Mexico 87545

A. J. Iverson
National Securities Technologies, 182 East Gate Drive, Los Alamos, New Mexico 87544

G. S. Macrum
Special Technologies Laboratory, 6159 Keister Place, Goleta, California 93117

K. B. Morley and A. W. Obst
P-23, Los Alamos National Laboratory, P.O. Box 1663, Los Alamos, New Mexico 87545

R. T. Olson
P-22, Los Alamos National Laboratory, P.O. Box 1663, Los Alamos, New Mexico 87545

J. R. Payton
P-23, Los Alamos National Laboratory, P.O. Box 1663, Los Alamos, New Mexico 87545

P. A. Rigg
DE-9, Los Alamos National Laboratory, P.O. Box 1663, Los Alamos, New Mexico 87545

N. Routley
Atomic Weapons Establishment, Aldermaston, Reading, Berkshire RG7 4PR, United Kingdom

G. D. Stevens, W. D. Turley, and L. Veeser
Special Technologies Laboratory, 6159 Keister Place, Goleta, California 93117

W. T. Buttler
P-23, Los Alamos National Laboratory, P.O. Box 1663, Los Alamos, New Mexico 87545

(Received 11 April 2007; accepted 21 May 2007; published online 10 July 2007; publisher error corrected 11 July 2007)

This effort investigates the relation between ejecta production and shock-breakout pressure (P_{SB}) for Sn shocked with a Taylor shockwave (unsupported) to pressures near the solid-on-release/partial melt-on-release phase transition region. The shockwaves were created by detonation of high explosive (HE) PBX-9501 on the front side of Sn coupons. Ejecta production at the backside or free side of the Sn coupons was characterized through use of piezoelectric pins, optical shadowgraphy, x-ray attenuation radiography, and optical-heterodyne velocimetry. Ejecta velocities, dynamic volume densities, and areal densities were then correlated with the shock-breakout pressure of Sn surfaces characterized by roughness average of $R_a=16$ μin or $R_a=32$ μin.
 [DOI: 10.1063/1.2752130]

I. INTRODUCTION

Los Alamos National Laboratory (LANL) is actively engaged in the development of a model to predict the formation of micron-scale fragments ejected (ejecta) from shocked metal surfaces. Of particular importance are experiments that focus on the relation of ejecta production to the physical properties of the shocked material, the shock strength, and the shock temporal profile or pressure-time history.[1–3] Previous models relate properties such as surface defects, inclusions, and voids to the formation of ejecta upon shock breakout at the surface. These models predict that ejecta production is relatively independent of shock-breakout pressure (P_{SB}) at the surface of the material as long as the shock pressure is sufficient to overcome the yield strength of the material.[4–6] However, the models warn about a possible P_{SB} upper bound for applicability in predicting ejecta production. Localized melting and formation of hot spots have also been shown to contribute to ejecta formation.[7] Formulation of a model to predict ejecta production that includes these mechanisms has proven difficult thus far.

[a)]Electronic mail: mzellner@lanl.gov

The LANL ejecta model considers that the amount of ejecta is mainly related to the material's phase on release. If the shock pressure releases to a material phase of solid-on-release, the amount of ejecta produced is expected to be related to the defect volume of the surface and is not expected to eject much material: several hundred micrograms per square centimeter. When the shock pressure releases to a material phase of partial melt-on-release,[8,9] it is estimated to eject up to $\times 10$ the amount of fragments that would be seen from a shock pressure that releases to a solid phase. These numbers are nominal, and may be higher or lower, but that is the motivation for much of our effort: ejecta model development or material science.

The experimental effort supporting the model development examines the correlation between ejecta production and P_{SB} for a solid/liquid phase transition region in Sn. The effort is characterized by ejecta measurements made from Sn targets shocked to pressures that release to states near the onset of partial melt-on-release throughout pressures that release to states with a significant fraction of solid/liquid phase. Further, the experiments focus on ejecta production from shocked Sn surfaces for two surface finishes. The purpose of using two finishes was to improve our understanding of instability driven ejecta production mechanisms that propagate from surface defects, inclusions, and voids upon shock breakout at the material surface.

To measure ejecta properties such as the dynamic volume density, areal density, and impact pressure, we fielded two types of piezoelectric probes,[2,3,10] optical shadowgraphy,[11,12] and x-ray attenuation.[12,13] Additionally, optical-heterodyne velocimetry (OHV) measured the asymptotic free-surface velocity, peak free-surface jump velocity, and shock-breakout time.[14,15] The use of multiple diagnostic techniques to characterize the ejecta provided redundancy and allowed for comparison of ejecta properties measured in different ways.

II. EXPERIMENT

Experiments were executed in a high explosive (HE) test chamber at the Special Technologies Laboratory in Santa Barbara, CA. Ejecta were produced when the HE shock released at the Sn-vacuum interface. The high explosive used was PBX-9501 (cylindrical pellets 12.7 mm in height by 12.7- or 19.05-mm diameter), which was press-fit to the front side of a Sn target. Detonation of the HE caused an unsupported or Taylor wave pressure profile in which the peak pressure decays with time, and therefore with travel distance of the shockwave in the Sn [Figs. 1(a) and 1(b)]. As a result of the HE geometry, shock breakout is mostly flat in the central few millimeters of the target and curvature gradually increases at larger distances from the center.

The Sn targets (ESPI, 99.99%+ purity) were cylinders of either 40.0- or 50-mm diameter (50 mm targets were used with the 19.05 mm diameter HE). The Sn targets' thickness for each shot was varied to adjust the shock-breakout pressures. Target thicknesses of $\tau \in \{2.0,\ 2.5,\ 3.0,\ 3.5,\ 4.0,\ 4.5,\ 6.0\}$ mm resulted in a P_{SB} range of approximately 210 to 285 kbar. These pressures released to material states thought to be partially melted.

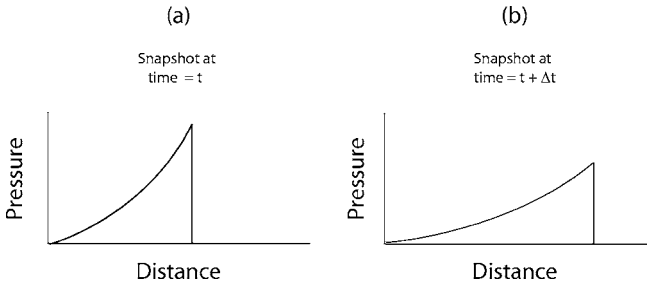

FIG. 1. Snapshots of (a) the pressure profile within a metal from a typical Taylor (unsupported) wave created by detonation of HE and (b) the pressure profile after some elapsed time Δt. Our experiments utilized targets of different thicknesses to take advantage of the decrease in peak shock pressure with increased time (or travel distance). This allowed us to correlate different shock-breakout pressures (P_{SB}) with ejecta production.

The backside or Sn-vacuum interface side of the Sn targets were prepared with a "fly-cut" machine finish, resulting in a series of "saw-tooth" or triangular grooves across the target surface. Two different finishes, one characterized by a surface roughness average $(R_a)=32\ \mu$in and the second by $R_a=16\ \mu$in as defined by ASME standards,[16] were used throughout the experiments. To minimize and control relevant variables such as the groove half-angle, the same tool was used to machine both surface finishes.[17]

Figure 2 schematically shows the geometry and diagnostics used for the experimental series. The Sn target, piezoelectric pins, and OHV probe were contained inside a package under vacuum of 2–5 Torr, inside the test chamber. The test chamber included two replaceable poly(methylmethacry-

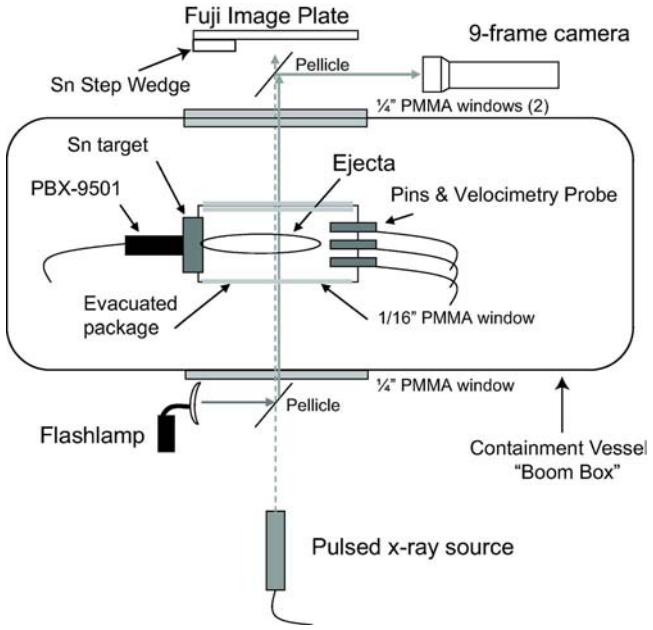

FIG. 2. Schematic of the experimental setup used to acquire data at NSTec./STL. Ejecta created from detonation of HE PBX-9501 on the back side of a Sn target was simultaneously measured using piezoelectric pins (pin heights nominally 20 mm), radiography, and optical shadowgraphy. Additionally, optical heterodyne velocimetry was used to measure the shock breakout time and make velocity measurements of the free-surface.

late) windows (often damaged by debris from the explosion) positioned perpendicular to the target face, allowing for use of both optical shadowgraphy and x-ray radiography. All diagnostics and the HE detonation were initiated from a central source using varying lengths of M17/84-RG223 coaxial cable. Time-domain reflectometry was used to measure signal delay times for the various lengths of cable. To obtain accurate cross timing of the experimental diagnostics, the final timing diagram accounted for these measurements, along with measured internal instrument and optical fiber length delays.

A. Piezoelectric pins

Charge accumulation in piezoelectric material results from formation of electric dipoles as the material is subject to mechanical distortion (strain).[18–20] The result of compression of a piezoelectric crystal from particle impact, in the absence of an external electric field, follows the equation

$$D_i = d_{ij}\sigma_j, \tag{1}$$

where D_i is the charge density, d_{ij} is the piezoelectric strain coefficient, and σ_j is the applied stress.[21] For uniaxial compression $(i=j)$, the applied stress is related to the measurable time-dependant voltage $V(t)$ across an impedance R by

$$\sigma \approx \frac{D_i}{d_{ii}} = \frac{1}{d_{ii}}\frac{Q}{A} = \frac{1}{d_{ii}}\frac{1}{A}\int_{t_o}^{t} dt\frac{V(t)}{R}, \tag{2}$$

where Q is the accumulated charge and A is the area that undergoes the stress. When using piezoelectric materials to characterize ejecta, the applied stress on the piezoelectric crystal can also be related to a change in momentum of the impacting ejecta

$$F(t) = \frac{dp}{dt} \approx m\frac{du(t)}{dt} = m\frac{\partial u}{\partial x}\frac{\partial x}{\partial t}$$

$$= mu(t)\frac{\partial u}{\partial x} \approx \frac{mu^2(t)}{\Delta x} = A\rho^*(t)u^2(t) \tag{3}$$

so

$$\sigma = \frac{F(t)}{A} = \rho^*(t)u^2(t) = P(t), \tag{4}$$

where $F(t)$ is the force, p is the momentum, m is the mass, u is the ejecta velocity, ρ^* is the ejecta dynamic volume density,[22] and $P(t)$ is the pressure as a function of time. Combining Eqs. (2) and (4) we find that

$$P(t) = \frac{F(t)}{A} = \int dt\frac{V(t)}{d_{ii}AR}, \tag{5}$$

and

$$\frac{dF(t)}{dt} = \frac{V(t)}{d_{ii}R}. \tag{6}$$

Equation (4) allows for ρ^* to be calculated if both the stress and velocity are known. However, to derive the equations that calculate the applied stress we assume: (1) ejecta are created instantaneously at shock breakout; (2) the interaction between the ejecta and the piezoelectric pin surface is fully inelastic; (3) the compression of the piezoelectric crystal is small; and (4) the ejecta mean-free path is long so that the ejecta do not undergo multiple scattering.

The piezoelectric pins themselves are characterized by a 1.27 mm diameter, $y+36°$-cut lithium niobate (LN) piezoelectric crystal of 0.5 mm thickness mounted to the end of a 25.4 mm long brass rod of the same diameter using silver epoxy. This assembly is encased in Kynar, which served as insulation, and inserted into a 2.35 mm diameter brass housing. Finally, a thin copper foil is applied over the crystal to complete the electrical circuit. The piezoelectric pins were purchased from Dynasen, Inc. and are characterized by a rise time on the order of tens of nanoseconds.[23] The LN piezoelectric crystal used is characterized by $d_{ii}=24.8$ pC/N, and a fail pressure of ≈ 6 kbar,[23] as inferred from "quasistatic" tests where the compression of the crystal is slow.

Some pins used in these experiments were altered by LANL to include 1/4 mm thick Ti foil and a 1/3 mm foam buffer, as well as a mask. The altered pins are referred to as lithium niobate masked and shielded (LN-M).[3] The LN-M pin signals were delayed by the shock travel time in the buffers and by a position offset of the crystal. These delays were equivalent to that which would have resulted from an additional 0.413 mm of travel distance of the ejecta relative to an unbuffered pin.

Depending on the diameter of the nominal shock-breakout area on the Sn surface, LN or both LN and LN-M piezoelectric pins were used for ejecta characterization. These piezoelectric pins technologies, as compared with other piezoelectric materials such as ferroelectric lead zirconate titanate, were selected based on their enhanced performance when measuring ejecta created from shocks with P_{SB} typical of these experiments.[3,10] In all cases, the piezoelectric pins were mounted with their axis normal to the target at a distance ≥ 20.0 mm from the target surface. The pin offset made the ejecta paths long enough to approximate the asymptotic velocities from their times of flight. The offset also spread the ejecta arrival times at the pins, reducing the maximum stress on the pins as the ejecta cloud undergoes self-similar expansion. If the pin stress is too great, it is plausible that the piezoelectric material could be driven into a region of plastic deformation instead of the desired region of elastic deformation and may preclude the pin's proper operation.[3]

To cover their full dynamic range, each pin output was divided across multiple recording channels that ranged in sensitivity from 0.5 to 80 V. A locally developed software package, eXtreme Las Vegas,[24] was used to correct the recorded signals for base line offsets, scale the signals according to their splitting ratios and electrical attenuation, and recombine the data into a single composite trace.

B. Optical shadowgraphy

Optical shadowgrams of the shock experiments were captured using a high-speed nine-frame camera.[2,11] The camera's field-of-view was oriented perpendicular to the axis of shock propagation as displayed in Fig. 2. A Xe flashlamp

provided illumination during the experiment. The exposure time of each frame was ≈150 ns. The first three frames were separated by 0.3 μs to capture shock breakout and the remaining six frames were separated by 1.5 μs to record the experiment's duration. Prior to each experiment, a "static" image was captured to correct the dynamic images for background and fixed pattern noise. For ease of data interpretation, a grid depicting distance was overlayed on the images. The grid was spatially calibrated using the distance between the piezoelectric pins and target surface.

C. X-ray attenuation

An x-ray attenuation radiograph of each experiment was captured using a pulsed x-ray source in combination with a Fuji image plate (BAS-IPMS2025) and a Fuji FLA-7000 scanner.[2] The radiograph was acquired at a preselected time after shock breakout and imaged the backsurface of the target. This was accomplished by triggering the x-ray source capacitors using an externally controlled timing circuit. A silicon diode, commonly timed with the optical shadowgraphy and piezoelectric pins, was placed near the x-ray head to monitor the x-ray pulse, allowing for accurate cross timing of the radiograph with other diagnostics.

A Sn step wedge of ten step thicknesses, ranging from 0.0254 to 1.8288 mm, was placed in front of the image plate so that it would not disrupt the experiment's field-of-view. Radiograph intensities from the known step wedge thicknesses were fit with a double exponential function to calibrate the intensity of the radiograph with the areal density of Sn. Further, an Abel inversion was utilized to extract the areal density for comparison and validation with piezoelectric pin data.

III. RESULTS

A. Piezoelectric pin results

Figure 3(a) shows the voltage vs time (the experimentally measured signal), Fig. 3(b) shows the corresponding pressure vs normalized velocity (u/u_{fs}, where u_{fs} is the free surface velocity), and Fig. 3(c) shows the corresponding areal density vs normalized velocity for the $\tau=2$ mm, $R_a=32$ μin Sn target. As described by Eq. (6), the measured voltage in Fig. 3(a) is related to the time derivative of the force from ejecta and metal fragment impact on the piezoelectric pin surface. Figure 3(a) displays two important features: the onset of voltage change and the time at which the piezoelectric pin was driven to its failure voltage of ≈70 V. The first feature indicates detection of the fastest ejecta and the later is an indication of the sample free-surface arrival, or a very dense layer of material, striking the pin. This information, combined with the known pin offset from the targets, allows estimation of the ejecta velocity, u_{ej}, and and the free surface velocity, u_{fs}. The signals measured between these two features are used to calculate the ejecta areal density, dynamic volume density, and pressure.

From Figs. 3(b) and 3(c) it is evident that there is good agreement between the two LN pins. This indicates that the pins were measuring similar phenomena, as expected if the ejecta cloud is roughly uniform and cylindrically symmetrical. Additionally, common features in the higher-velocity portions of both the LN and LN-M pressure vs velocity indicate a similar response between the two technologies. The LN piezoelectric pins, however, resulted in a higher pressure measurement and therefore areal density calculation. Calibration of the LN-M pins using $d_{ii}\approx 13-16$ pC/N (Ref. 3) allows a quantitative comparison between the two technologies. It is also evident that the LN-M pins act to smooth the signal response. Both phenomena are a direct effect of the shielding modification.

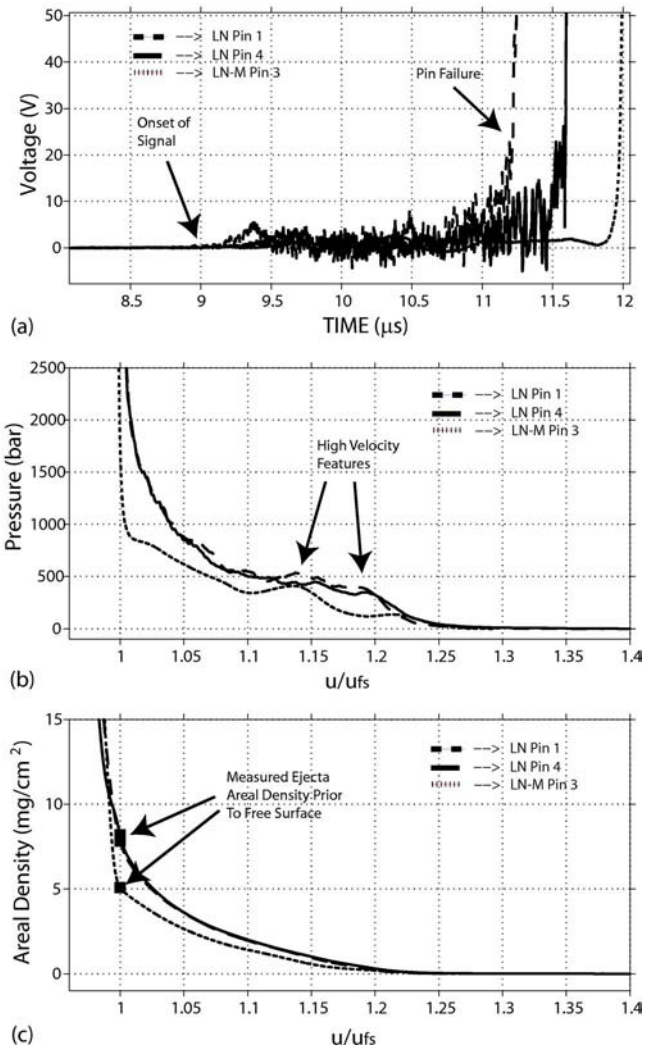

FIG. 3. (a) Voltage vs time, (b) pressure vs normalized velocity u/u_{fs}, and (c) areal density vs normalized velocity measurements recorded by the piezoelectric pins for a $\tau=2$ mm, $R_a=32$ μin Sn target shocked by HE PBX-9501 ($P_{SB}\approx 275$ kbar).

It is important to note the lack of intense peaks and clipping in the voltage vs time plot [Fig. 3(a)] during the region of ejecta measurement. Because the crystal pressures were well below the ≈6 kbar failure pressure of LN [Fig. 3(b)], it appears that the LN and LN-M pins were not "overdriven" during these particular ejecta measurements.[3] If overdriving conditions exist, the piezoelectric pin may overestimate results of the pressure and ejecta densities, or fail early, i.e., prior to arrival of the free surface.

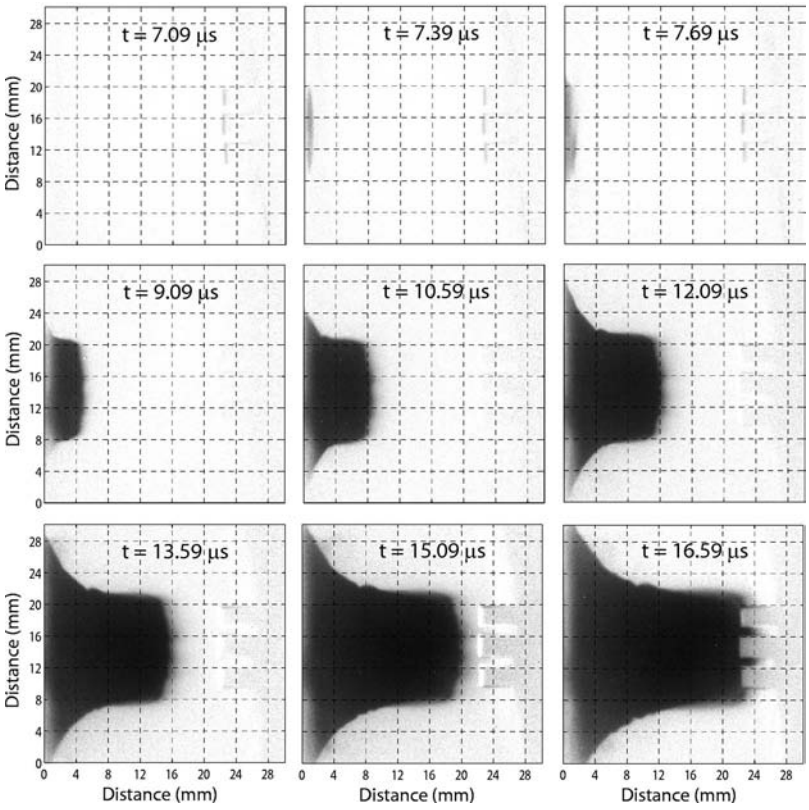

FIG. 4. Optical shadowgraphs taken with the nine-frame camera of a τ=2 mm, R_a=32 μin Sn target shocked by HE PBX-9501 ($P_{SB} \approx 275$ kbar). These images were used to measure various leading edge/fastest ejecta velocities and to estimate shock breakout time. The images often capture asymmetries in the ejecta clouds. In the final frame, the opaque material has impacted the pins.

B. Optical shadowgraphy results

Figure 4 shows the nine-frame camera images for the τ =2 mm, R_a=32 μin Sn target shocked to $P_{SB} \approx 275$ kbar. These images indicate shock breakout at ≈7.2 μs followed by production of a relatively symmetric ejecta front. The fastest moving ejecta appear further in progression as a "hazy cloud" preceding the main ejecta cloud.

The outlines of the piezoelectric pins (seen to the far right) were used to calibrate distance, which in turn allowed for ejecta velocity estimation. This is typically performed by plotting the distance of the leading edge of the fragments vs time and using a linear fit to extract the velocity. For this particular shot, the slope gives a velocity of 2.54 mm/μs for the fastest ejecta. Calculation of the fastest ejecta velocity via optical shadowgraphy typically agrees well with that from radiographic results, which gave ≈2.6 mm/μs for the same shot (see Fig. 8).

Figures 5 and 6 show sample nine-frame camera images of asymmetric shock events from: τ=4.5 mm, R_a=16 μin, $P_{SB} \approx 215$ kbar and τ=3.5 mm, R_a=32 μin, $P_{SB} \approx 225$ kbar Sn targets. These images display the capability of optical shadowgraphy to assist in the interpretation of shock events that, when considered in the absence of this diagnostic, may be misinterpreted. In particular, Fig. 5 shows formation of a possible particle jet and dense layers of material, and Fig. 6 shows a nonuniform ejecta front. Both phenomena captured by the nine-frame camera were confirmed

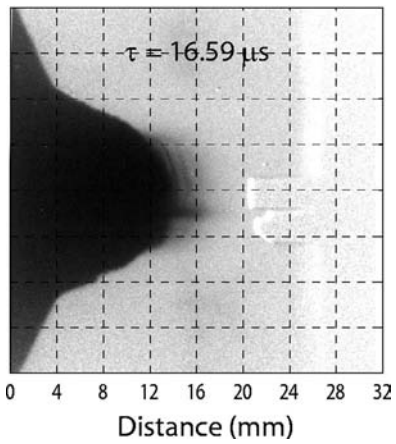

FIG. 5. Asymmetric features captured by the nine-frame camera of dense ejecta layers and perhaps jet formation from the τ=4.5 mm, R_a=16 μin target shocked by HE PBX-9501 ($P_{SB} \approx 215$ kbar).

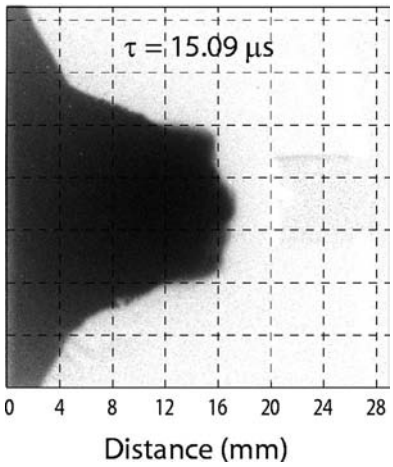

FIG. 6. Asymmetric features captured by the nine-frame camera of nonuniform ejecta distribution from the τ=3.5 mm R_a=32 μin target shocked by HE PBX-9501 ($P_{SB} \approx 225$ kbar).

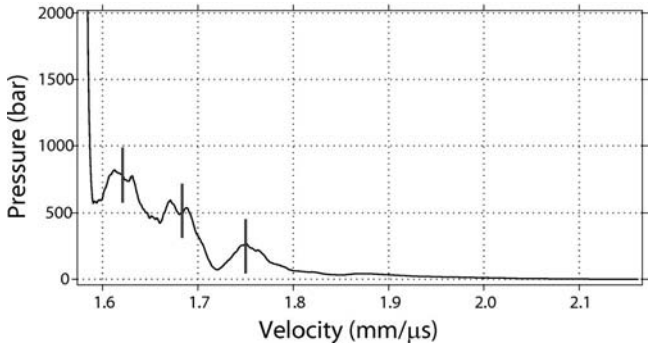

FIG. 7. Overlay of LN piezoelectric pin pressure spectrum with velocities of three dense bands derived from optical shadowgraphy (Fig. 4) of a τ =4.5 mm, R_a=16 μin target shocked by HE PBX-9501 ($P \approx 215$ kbar). These data were used to check the validity of the diagnostics for making ejecta measurements within a single shot.

by fluctuations in the piezoelectric pin pressure vs time measurements or by particle velocity measurements acquired by the multiple diagnostic methods. This is discussed further in Sec. III D.

C. Radiographic results

A single radiograph was taken for each Sn target shocked with HE. The images were acquired ≈ 6 μs after shock breakout (estimated from both the OHV jump and optical shadowgraphy). The radiographs typically reveal an ejecta front, a hazy cloud of ejecta, shadows outlining the piezoelectric pins and OHV probe, and a Sn step wedge used to calibrate the x-ray intensity to the Sn areal density. Similar to the optical shadowgraphy, the piezoelectric pin distance from the target was used to calibrate distance and therefore obtain velocities from the radiograph. Unlike optical shadowgraphy, however, the radiographs give a clear view of the free surface due to the ability of x-rays to penetrate through the ejecta cloud.

D. Diagnostic comparison of measured ejecta properties

It is important to compare measurements between the multiple diagnostics within a single shot. These comparisons validate the individual diagnostics for making measurements of ejecta. The ability of the nine-frame camera to image asymmetric features provides an excellent opportunity for such comparisons. In addition to the possible jet, Fig. 5 shows three distinct alternating high and low density "sheets" of material traveling in front of the free surface. Figure 7 displays the pressure vs velocity spectrum obtained for a LN piezoelectric pin on the same shot. Overlaid on Fig. 7 are three vertical lines corresponding to the velocities of the three ejecta sheets seen in the optical shadowgraphs. Correlation between the piezoelectric pin pressure spectrum and the sheets velocities from the optical shadowgrams confirms the two diagnostics are measuring similar phenomena.

Another comparison is made with ejecta dynamic volume density measurements between x-ray attenuation and the piezoelectric pins. Figure 8 shows the ejecta dynamic volume density measured by both techniques for the τ =2 mm, R_a=32 μin target plotted against absolute velocity and normalized to the free-surface velocity. Overall, the two diagnostics show good agreement. One exception is that both the LN and LN-M piezoelectric pins display features at higher velocities that are not detected by the radiograph. This shows that the piezoelectric pins are sensitive to lower amounts of areal mass than our most sensitive x-ray measurements.

IV. DISCUSSION

A. Free-surface velocity and pressure

In the present experiments, P_{SB} was estimated from u_{fs} measurements. Use of multiple diagnostics allowed for u_{fs} to be measured in many ways, resulting in slight variations in the determination of P_{SB}.

Optical heterodyne velocimetry provided two distinct measurements of the u_{fs}: the velocity derived immediately after shock breakout (denoted OHV breakout velocity) and the relatively constant velocity that the free surface approaches with increasing time (denoted OHV asymptotic velocity). In addition, u_{fs} can be derived from the free-surface time of arrival at the piezoelectric pins relative to shock release time. In this situation, both the pin offset distance and time of shock breakout relative to the recorded pin signal must be well known. In the present experiments, the latter can be inferred from either the jump in the OHV velocity[15] or through optical shadowgraphy. An additional estimate of u_{fs} can be obtained by radiography. This method derives the velocity through observation of the distance the free surface has traveled over the time interval from breakout to image time. Here the time of shock breakout, as well as the elapsed frame time, must be well known.

Figure 9 displays the calculated P_{SB} for Sn targets of multiple thickness using u_{fs} from OHV and piezoelectric pin methods described earlier. Typically, the radiographs tend to give relatively high u_{fs} estimates and are therefore not included in Fig. 9. This may be related to the inability to precisely define the edge of the free surface in the radiographs, therefore, velocities may be unintentionally measured from ejecta and dense material moving slightly faster than the free surface. Variation may also result from unresolvable timing issues. For the region where the Sn is believed to result in a significant portion of surface melt ($P_{SB} > 230$ kbar), u_{fs} from OHV measurements immediately after breakout and from the piezoelectric pin failure tend to agree to within 1%. Similar to optical shadowgraphy and x-ray attenuation, slight discrepancies may be attributed to differences in the ejecta penetrability of the two diagnostics.[25] For the region near the onset of the solid-on-release/partial melt-on-release phase transition, u_{fs} from the piezoelectric pin failures tend to agree better with the OHV asymptotic u_{fs}, which typically reports the lowest velocity measurement. The agreement between the OHV asymptotic u_{fs} and that estimated from piezoelectric pin failures at lower pressure is attributed to increasing effects of material strength as the pressure nears the solid-on-release/partial melt-on-release phase transition. This is not as evident at pressures that result in a significant portion of surface melt. However, because ejecta are assumed to be

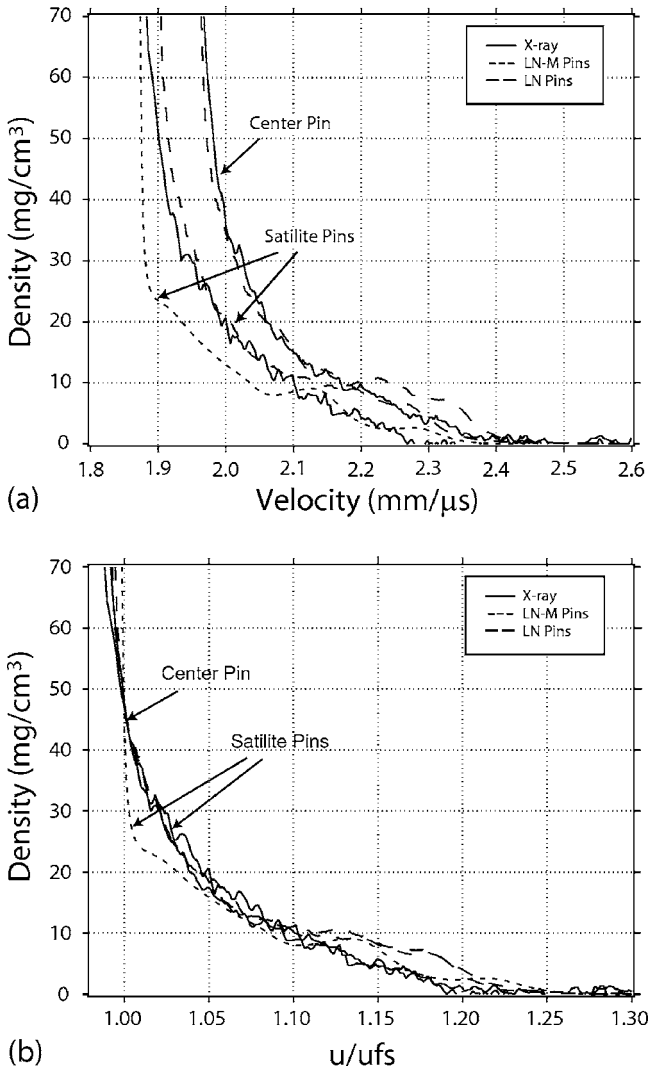

FIG. 8. Overlay of ejecta volume density as measured by LN and LN-M piezoelectric pins and x-ray attenuation radiographs plotted vs (a) velocity and (b) normalized to the free-surface velocity for a $\tau=2$ mm, $R_a=32$ μin target shocked by HE PBX-9501. These data were used to check the accuracy of the diagnostics and validate the technique for making ejecta measurements within a single shot.

created instantaneously at shock breakout, we regard the OHV measurement immediately after breakout to be the most accurate velocity measure for calculating ejecta production. This measurement is consistently to infer conclusions.

B. Areal density and pressure

The formation of ejecta by shockwave release at a metal-vacuum interface is strongly dependent on the local material defect properties as well as the shock strength and its temporal evolution. One possible contribution to ejecta formation is microjets from pits, scratches, or grooves.[4,5,7,26] Inclusions and voids within the material can result in the formation of hot spots and metal fragmentation at grain boundaries.[7,27] In addition, the release-to-partial-liquid state has been shown to significantly increase the amount of ejecta compared to release-to-solid.[6,7,13] For the latter, the shock strength and temporal profile define the material state on release.[28–32]

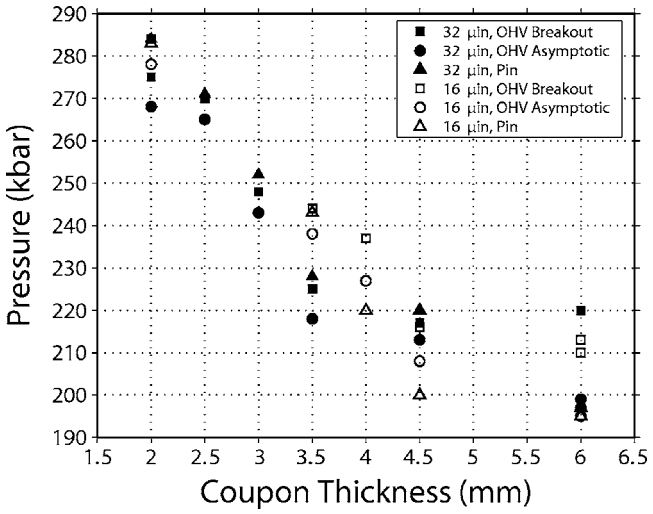

FIG. 9. Comparison of target thickness and shock breakout pressure (P_{SB}) for targets shocked with HE PBX-9501. The pressure was calculated using free-surface velocity (u_{fs}) measurements from OHV and piezoelectric pin failure. OHV provided two distinct measurements of the u_{fs}: the velocity derived immediately after shock breakout (denoted OHV breakout velocity) and the relatively constant velocity that the free surface approaches with increasing time (denoted OHV asymptotic velocity). Variations between velocity measurements of the different methods increase as the targets become thicker. This is attributed to increased effects of material strength as P_{SB} decreases toward the region resulting in a solid phase upon shock breakout at the free surface of the target. Because ejecta are assumed to be created instantaneously at shock breakout, we regard the OHV measurement immediately after breakout to be the most accurate velocity for calculating P_{SB} relating to ejecta production.

One convenient parameter to quantify the amount of ejected fragments is the cumulative areal density defined as the value of the areal density (dm/dA, denoted ρ_a) evaluated at the free surface. Figure 10 plots the cumulative ejecta areal density vs P_{SB} of (a) LN pins for Sn surfaces characterized by $R_a=32$ μin, (b) LN-M pins for Sn surfaces characterized by $R_a=32$ μin, (c) LN pins for Sn surfaces characterized by $R_a=16$ μin, and (d) LN-M pins for Sn surfaces characterized by $R_a=16$ μin. In general these plots show two distinct production response regions: the region where $P_{SB}>220$ kbar, which displays relatively constant ejecta production, and the region where $P_{SB}\lesssim 220$ kbar, where the cumulative areal density appears to decrease sharply with decreasing pressure. In the region where $P_{SB}>220$ kbar, the apparent linear offset between measurements with LN vs LN-M plots for similar surfaces [Figs. 10(a) and 10(b)] relates the technology differences between LN and LN-M pins. However, a true linear offset of ejecta areal density exists related to surface preparation [Figs. 10(a)–10(d)].

A similar observation was made concerning ejecta areal densities measured from Pb using a supported plane wave to span pressures above and below surface melt-on-release.[6] Similar to the Pb work, the shock-breakout pressure corresponding to the steep rise in ejecta production for Sn correlates well with the onset of what is believed to be melt-on-release.[28–32] A slight increase in the ejecta prior to the onset of equilibrium melt has previously been attributed to the inability of temperature to reach equilibrium within the nanosecond time scale of the shock event, therefore resulting in localized melting or evaporation on the surface.[6] The

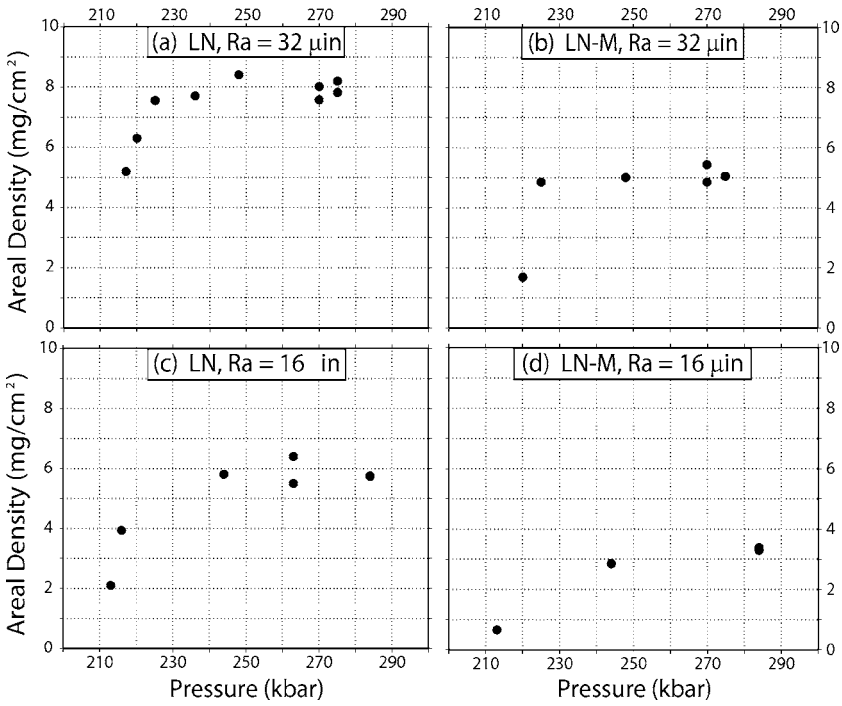

FIG. 10. Cumulative ejecta areal density vs shock-breakout pressure of (a) LN pins for Sn surfaces characterized by R_a=32 μin, (b) LN-M pins for Sn surfaces characterized by R_a=32 μin, (c) LN pins for Sn surfaces characterized by R_a=16 μin, and (d) LN-M pins for Sn surfaces characterized by R_a=16 μin These plots display a steep rise in ejecta production at the lower pressures followed by a region of relatively constant ejecta production for $P_{SB}>220$ kbar. Considering the regions of relatively constant cumulative ejecta areal density, a true linear offset exists for surfaces characterized by R_a=32 μin compared with that characterized by R_a=16 μin. However, the apparent offset between amounts of ejecta detected with LN vs LN-M pins for surfaces characterized by a single R_a is related to a decrease in sensitivity of the LN-M pins (13–16 pC/N) compared to the LN pins (24.8 pC/N) (Ref. 3).

slight increase can also be attributed to the inability to precisely measure shock pressures, therefore making it difficult to correlate a particular shock pressure with a phase transition such as the solid to liquid phase transition. The present work is different from these works in that we investigate a Taylor wave shocks, and we probe many pressures within the region of "partial melt." These differences resulted in detection of a region with relatively constant ejecta production separated from a region of increasing ejecta production near the onset of melt-on-release.

Overall, these results suggest that additional mechanisms, correlated with pressures resulting in the onset of partial melt-on-release, appear to play a dominant role in ejecta production throughout the region examined in Sn. However, one must also acknowledge that multiple competitive processes for ejecta production may be occurring simultaneously. dominance of the relative effectiveness

C. Areal density and surface roughness

Effects of surface roughness on ejecta production have been previously assessed by examining the "jetting factor" (R), i.e., the ratio of ejecta mass to the surface defect volume, V_d (Refs. 2 and 4)

$$\text{ratio} \equiv R \equiv \frac{M_{\text{ej}}}{\rho V_d}, \tag{7}$$

where M_{ej} is the mass of the ejecta and ρ is the material density (7287 mg/cm^3 for Sn). Equation (7) implies that if the defect volume of the sample increases, holding all other parameters constant, then the amount of ejected fragments should also increase.

Vogan *et al.*[2] noted that for surfaces characterized by perfect triangular fly-cut grooves, R could be expressed in terms of the "effective depth," ρ_a/ρ, and the depth of the fly-cut grooves, $4R_a$ (Ref. 33)

$$\text{ratio} = R = \frac{\rho_a}{\rho}\frac{1}{2R_a}, \tag{8}$$

where ρ_a is the cumulative areal density. This expression was calculated for regularly spaced isosceles triangular grooves, however, surface profiles of the samples used in this study indicate that this is not always a valid assumption. As a result, the value of 2 in the denominator of Eq. (8) is not accurate. Using surface profilometry, we were able to estimate the volume represented by the surface defects, V_d for each finish type. These volumes were calculated using the deviation from a plane situated parallel to the surface at the height of the maximum surface peak (denoted $V_{d_{\text{pp}}}$). The calculated $\langle V_{d_{\text{pp}}}\rangle$ for surface finishes R_a=16 and R_a=32 μin are 2.04×10^{-4} and 2.54×10^{-4} cm^3 (per unit surface area), respectively. Using these results, we estimate that the factor of two in the denominator of Eq. (8) should be 4.7 and 3.2 for finishes R_a=16 and R_a=32 μin, respectively. These results predict that the amount of material ejected from the surface with a R_a=32 μin finish should be a factor of 1.24 times greater than that from the R_a=16 μin finish surface. A second estimation of V_d was calculated by summing the average defect area, $\langle A_d\rangle$, defined from a line at the maximum of each individual length-wise scan across the sample, multiplied by the width element (denoted V_{d_A}). This method resulted in $\langle V_{d_A}\rangle \approx 1.59\times10^{-4}$ and 2.05×10^{-4} cm^3 for R_a=16 μin and R_a=32 μin finishes, respectively, which correlates to an effective R_a multipliers of 3.9 and 2.6, respectively. These results predict that the amount of fragments ejected from the surface with the R_a=32 μin finish should be a factor of $\times$1.29 greater than those characterized by a R_a=16 μin finish. The above values are summarized in Table I. For LN pins at $P_{\text{SB}}\gtrsim220$ kbar, measurements of ρ_a for Sn surfaces characterized by the R_a=32 μin finish were a factor of $\approx$ $\times$1.3 higher than the surface characterized by a R_a

TABLE I. Average defect volumes and corresponding effective R_a multipliers for surfaces characterized by R_a=32 μin and R_a=16 μin finishes. Two methods were used to estimate the defect volume (V_d). The first calculated V_d from a perfect plane situated parallel to the surface at the height of the maximum surface peak (denoted $V_{d_{pp}}$). The second method calculated V_d by summing the average defect area, $\langle A_d \rangle$, of many length-wise scans across the sample surface, multiplied by the width element (denoted V_{d_A}).

Nominal surface roughness average (R_a, μin)	Analysis method	Average defect volume ($\langle V_d \rangle$, cm^3, per unit surface area)	Effective R_a multiplier	Standard deviation of R_a multiplier
16	$V_{d_{pp}}$	2.04×10^{-4}	4.7	0.4
32	$V_{d_{pp}}$	2.54×10^{-4}	3.2	0.4
16	V_{d_A}	1.59×10^{-4}	3.9	0.5
32	V_{d_A}	2.05×10^{-4}	2.6	0.2

=16 μin For LN-M pins, the factor was $\approx\times1.6$. Lack of sufficient low pressure shots prevented similar calculations for $P_{SB}\leq220$ kbar.[34]

Further examination of the relation between ejecta production and the defect volume can be made by considering the ratio values (R) of Eqs. (7) and (8). Table II displays R using the effective R_a multiplier derived from $\langle V_{d_{pp}} \rangle$ for various shots ranging in pressures from P_{SB}=210 to 285 kbar. Analysis of shots for $P_{SB}>220$ kbar indicates that both the 32 μin finish and the 16 μin finish result in $\langle R \rangle$=4.2 as measured with LN pins. Similar analysis with LN-M pins result in $\langle R \rangle$=2.7 and 2.3 for surfaces characterized by the 32 μin finish and the 16 μin finish, respectively (these values agree with the LN values when corrected for the decreased sensitivity of the LN-M pins). For $P_{SB}\leq220$ kbar, R sharply decreases. These results do not match models that attempt to predict ejecta production based solely on instabilities propagating from surface defect volume,[4,5] where R should be near unity (we note that if R were unity, we would expect ρ_a=1.67 and 139 mg/cm^2 for surfaces characterized by R_a=32 μin and R_a=16 μin finishes, respectively, as calculated with $V_{d_{pp}}$=3.2 and 4.7, respectively). Instead these R values support a model similar to that of LANL where the combination of shock pressure and surface finish result in greater amounts of ejecta production.

These results indicate that surface defects play a significant role in ejecta production upon shock breakout, but additional processes may also contribute to ejecta production at pressures that result in partial melt-on-release, as the jetting factor changes with pressure while the surface defect volume remains constant.

TABLE II. Comparison ratios of ejecta mass to surface defect volume (i.e., jetting factor, R) for multiple surfaces shocked with a Taylor wave near the solid-on-release/partial melt-on-release phase transition region and continuing throughout the region of partial melt-on-release. Ratios were calculated using a multiplier of R_a equal to 3.2 or 4.7 for surfaces characterized by R_a=32 μin and R_a=16 μin, respectively. These multiplier values were derived from an estimation of the defect volume (V_d), which was calculated from a perfect plane situated parallel to the surface at the height of the maximum surface peak.

Nominal surface shock breakout pressure (kbar)	Roughness average ρ_a (mg/cm^2) (LN:LN-M)	(R_a)=32 μin $R=\frac{\rho_a}{\rho}\frac{1}{3.2R_a}$ (LN:LN-M)
275	7.8:5.1	4.1:2.8
275	8.2:*	4.4:*
270	7.6:5.4	4.0:2.9
270	8.0:4.9	4.3:2.6
248	8.4:5.0	4.4:2.6
225	7.6:4.9	4.0:2.6
236	7.7:*	4.1:*
217	5.2:*	2.7:*
220	6.4:1.7	3.4:0.9
Nominal surface shock breakout pressure (kbar)	**Roughness average ρ_a (mg/cm^2) (LN:LN-M)**	**(R_a)=16 μin $R=\frac{\rho_a}{\rho}\frac{1}{4.7R_a}$ (LN:LN-M)**
284	5.7:3.3	3.9:2.4
284	5.8:3.4	4.2:2.5
263	5.5:*	3.9:*
263	6.4:*	4.6:*
244	5.8:2.9	4.2:2.0
216	3.9:*	2.8:*
213	2.1:0.7	1.5:0.5

V. CONCLUSIONS

Ejecta densities were measured for multiple Sn targets shocked to pressures near the threshold for partial melt on release up to pressures resulting in a significant fraction of surface melt. Multiple diagnostics, including two types of piezoelectric pins, optical shadowgraphy, radiography, and OHV, were used to measure various ejecta and shock properties. The agreement between diagnostics within a single shot demonstrates the validity of the technologies for making such measurements.

Measurements of cumulative areal density for Sn targets shocked with an unsupported (Taylor) wave and resulting in P_{SB} of 210–285 kbar displayed a steep rise in the amount of ejecta at the lower pressures followed by a region of relatively constant cumulative ejecta areal density. The shock-breakout pressures for the region of relatively constant ejecta spanned from $\approx$220 up to $\approx$285 kbar (the maximum P_{SB} tested).

In the region $220<P_{SB}\leq285$ (i.e., the region of relatively constant ejecta production), a linear offset was observed in the amount of fragments ejected for Sn surfaces that were characterized by different finishes. For measurements made with LN piezoelectric pins, the R_a=32 μin surfaces resulted in a factor of $\approx\times1.3$ more ejecta than for R_a=16 μin surfaces. For LN-M piezoelectric pins this factor was $\approx\times1.6$, which is within the uncertainty considering LN-M pins reduced sensitivities compared to that of LN. Additionally, the ratio of ejecta mass to surface defect volume, along the relatively constant regions, as measured by LN pins was $\langle R \rangle$=4.2 for both surfaces and as measured by

LN-M pins was $\langle R \rangle = 2.7$ and 2.3 for surfaces characterized by $R_a = 32$ μin and $R_a = 16$ μin finishes, respectively. These values decreased sharply for both LN and LN-M technologies when $P_{SB} \leq 220$ kbar.

ACKNOWLEDGMENTS

This work was suported by the U.S. Department of Energy. The authors acknowledge the contributions to these experiments by members of Los Alamos and Materials Science and Technology Divisions, citing in particular Robert D. Day and Felix P. Garcia (MST-7).

[1]W. T. Buttler, W. W. Anderson, and R. T. Olson, Report No. LA-UR-02–5211, 2002.
[2]W. S. Vogan, W. W. Anderson, M. Grover, J. E. Hammerberg, N. S. P. King, S. K. Lamoreaux, G. Macrum, K. B. Morley, P. A. Rigg, G. D. Stevens, W. D. Turley, L. R. Veeser, and W. T. Buttler, J. Appl. Phys. **98**, 113508 (2005).
[3]W. T. Buttler, M. B. Zellner, R. T. Olson, P. A. Rigg, R. S. Hixon, J. E. Hammerberg, A. W. Obst, and J. R. Payton, J. Appl. Phys., **101**, 063547 (2007).
[4]J. R. Asay, L. P. Mix, and F. C. Perry, Appl. Phys. Lett. **29**, 284 (1976).
[5]J. R. Asay and L. D. Bertholf, Report No. SAND-78–1256, 1978.
[6]J. R. Asay, Report No. SAND-76–0542, 1976.
[7]P. Andriot, P. Chapron, and F. Olive, AIP Conf. Proc. **78**, 505 (1981).
[8]Partial melt-on-release refers to a region of mixed solid and liquid material, not full melt-on-shock.
[9]C. Greeff, E. Chisolm, and D. George, Report No. LA-UR-05–9414, 2005.
[10]C. E. Lloyd, M. W. Greenaway, and W. G. Proud, AIP Conf. Proc. **845**, 1195 (2006).
[11]S. E. Barker, Electro-Opt. Syst. Design **4772**, 95 (2002).
[12]P. Elias and P. Chapron, in *Experimental Techniques for Measuring Mass Ejection from Shock-Loaded Metallic Sample*, edited by Y. M. Gupta (North-Holland Physics Publishing, Spokane, WA, 1985), p. 645.
[13]P. Andriot, P. Chapron, V. Lambert, and F. Olive, in *Influence of Melting on Shocked Free Surface Behavior Using Doppler Laser Interferometry and X-Ray Densitometry*, edited by J. R. Asay, R. A. Graham, and G. K. Straub (North-Holland Physics Publishing, Sante Fe, NM, 1983), p. 276.
[14]W. T. Buttler, S. K. Lamoreaux, F. G. Omenetto, and J. R. Torgerson, Report No. LA-UR-04–6453, 2004.
[15]O. T. Strand, D. R. Goosman, C. Martinez, and T. L. Whitworth, Rev. Sci. Instrum. **77**, 083108 (2006).
[16]Report No. ASME B46.1–2002, 2002.
[17]To reduce variables related to target fabrication, the materials are machined by the same individual in the materials science division (MST-7) of LANL, F. Garcia.
[18]D. J. Jones, S. E. Prasad, and J. B. Wallace, Key Eng. Mater. **122–124**, 71 (1996).
[19]J. Curie and P. Curie, Bull. Soc. Fr. Mineral. **3**, 90 (1880).
[20]J. Curie and P. Curie, Compt. Rend. **91**, 383 (1880).
[21]C. S. Speight, L. Harper, and V. S. Smeeton, Rev. Sci. Instrum. **60**, 3802 (1989).
[22]The dynamic volume density (ρ^*) is the apparent volume density that encompases the density of ejecta particles (similar to the density of pure Sn, 7.287 g/cm^3) as well as regions of empty space.
[23]Dynasen, www.dynasen.com, Goleta, CA.
[24]W. T. Buttler, A.-T. Nguen, C. Donahue, eXtreme Las Vegas LA-CC-06–030, 2003.
[25]The OHV ejecta signals are characterized by single wavelength Mie scattering. If the scattering cross section is strong enough, the OHV diagnostic may not even scatter light from the free surface.
[26]D. S. Sorenson, R. W. Minich, J. L. Romero, T. W. Tunnell, and R. M. Malone, J. Appl. Phys. **92**, 5830 (2002).
[27]B. L. Holian, T. C. Germann, J. Maillet, and C. T. White, Phys. Rev. Lett. **89**, 285501 (2002).
[28]P. Elias, P. Chapron, and B. Laurent, Opt. Commun. **66**, 100 (1988).
[29]D. Hayes, Los Alamos National Lab (private communication).
[30]C. Mabire and P. L. Hereil, AIP Conf. Proc. **505**, 93 (2000).
[31]C. Mabire and P. L. Hereil, J. Phys. IV **10**, Pr9 749 (2000).
[32]P. Chapron, P. Elias, and B. Laurent, in *Experimental Determination of the Pressure Inducing Melting in Release for Shock-Loaded Metallic Sample*, edited by S. C. Schmidt and N. C. Holmes (North-Holland Physics Publishing, Monterey, CA, 1987), p. 171.
[33]Equation (8) relates the defect volume of triangular fly-cut grooves, V_d, to $1/2 \times L \times W \times 4R_a$.
[34]We observe that analysis of the surface with optical profilometry showed the most common groove frequency for the 16 μin surface finish was a factor of ≈ 1.4 higher than the 32 μin surface finish. The correlation of increased groove frequency with an decrease in ejecta production over the pressures spanned is interesting and warrants further investigation.